Materials Today Communications 49 (2025) 114177

Contents lists available at ScienceDirect

Materials Today Communications

journal homepage: www.elsevier.com/locate/mtcomm

Electrospun membranes of polyhydroxybutyrate–niobium pentoxide as potential scaffolds for bone tissue engineering

Anna Raffaela de Matos Costa [a,1], Anna Valentino [b,c,1], Irene Bonadies [d,*], Yêda Medeiros Bastos de Almeida [e], Donatella Duraccio [f], Anna Calarco [b,c], Giovanna Gomez d'Ayala [d]

[a] School of Design, Management and Production on Technologies Northern Aveiro-ESAN, CICECO-Aveiro Institute of Materials, Estrada do Cercal, 4449, Santiago de Riba, Ul, Oliveira de Azeméis 3720-509, Portugal
[b] Research Institute on Terrestrial Ecosystems (IRET), National Research Council (CNR), Via Pietro Castellino 111, Naples 80131, Italy
[c] National Biodiversity Future Center (NBFC), Palermo 90133, Italy
[d] Institute of Polymers, Composites and Biomaterials (IPCB), National Research Council (CNR), Via Campi Flegrei 34, Pozzuoli 80078, Italy
[e] Department of Chemical Engineering, Federal University of Pernambuco, Cidade Universitária, Recife, PE 50670-901, Brazil
[f] Institute of Sciences and Technologies for Sustainable Energy and Mobility (STEMS), National Research Council (CNR), Strada delle Cacce 73, Torino 10135, Italy

ARTICLE INFO

Keywords:
Electrospinning
Polyhydroxybutyrate
Niobium oxide
Composites
Degradable scaffold
Bone tissue engineering

ABSTRACT

In recent years, the fabrication of biomimetic electrospun membranes has represented a promising approach for bone tissue engineering. In this study, electrospun composite fibers based on polyhydroxybutyrate (PHB) and different amounts of niobium oxide were developed, and the influence of Nb_2O_5 on physicochemical and biological properties was investigated. Electrospinning conditions were optimized, yielding nearly bead-free, randomly oriented fibers. SEM analysis revealed that Nb_2O_5 affected fiber size, reducing their diameters by approximately 16 %, whereas it did not influence membrane wettability, suggesting that the particles were embedded within the polymer matrix. FTIR-ATR analysis revealed physical interactions between Nb_2O_5 and PHB, mainly involving the amorphous phase. Furthermore, the incorporation of an increasing amount of Nb_2O_5 decreased PHB crystallinity and significantly enhanced tensile strength and Young's modulus, the latter reaching a value of 85.50 ± 0.15 MPa for PHB-Nb_2O_5 94/6 w/w (PHB-Nb6), three times that of pure PHB. Hydrolitic degradation study suggested that the presence of oxide slightly reduced membrane degradation rate in the early stage. All oxide-containing membranes showed no toxicity to hBMSCs and exhibited osteoinductive potential, with concentration-dependent increases in mineralization and ALP activity, peaking with PHB-Nb6. Finally, qRT-PCR analysis showed upregulated expression of osteogenic differentiation-related genes in hBMSCs cultured with PHB-Nb membranes.

1. Introduction

Injuries to bone tissue are widespread and result from several factors, including accidents, congenital diseases, and increased fragility associated with aging [1]. Bone tissue can heal naturally under normal physiological conditions in cases of minor injuries; however, in the case of large fractures involving surrounding tissues, natural bone remodeling alone is not sufficient [2]. In recent decades, tissue engineering has become a promising strategy for repairing damaged tissues and restoring their natural functions [3]. As for bone regeneration, an effective scaffold must accelerate bone formation while supporting remodelling to maintain bone quality [4]. In recent years, Guided Bone Regeneration (GBR) membranes have become widely used for bone tissue regeneration, offering efficient cell adhesion and proliferation to enhance bone defect repair [5–7]. These membranes must exhibit not only adequate mechanical properties to conform to the areas of bone defects, but also excellent biocompatibility and a suitable biodegradation profile to support cell growth and tissue reconstruction [8]. Moreover, they must allow for gas exchange while slowly degrading in the body as cell regeneration takes place and is replaced by regenerated tissue [9]. GBR

* Corresponding author.
E-mail address: irene.bonadies@cnr.it (I. Bonadies).
[1] These authors contributed equally to the work.

https://doi.org/10.1016/j.mtcomm.2025.114177
Received 16 June 2025; Received in revised form 30 September 2025; Accepted 25 October 2025
Available online 27 October 2025

membranes have garnered significant attention due to their high similarity to the extracellular matrix (ECM), as well as their high porosity and specific surface area, which promote cell growth and proliferation [10]. Compared to traditional scaffolds, the fibrous structures provide superior conditions for large-scale cell growth, highlighting the need for innovative approaches to design more bioactive fibrous materials. Among the various techniques employed to fabricate GBR membranes, electrospinning has garnered increasing interest and attention for applications in fields such as tissue engineering and drug delivery. Electrospun fibers can create 3D biomimetic structures with a multi-layered configuration and controlled pore sizes, mimicking the extracellular matrix of the human body [11]. Additionally, this approach enables the controlled incorporation of bioactive agents, thereby enhancing their capacity to promote bone regeneration. The porous structure of electrospun matrices facilitates the diffusion of nutrients and cell migration, contributing to the formation of new bone tissue.

The selection of material for the matrix development plays a key role, as it directly influences the properties and performance of the electrospun fibers. Different materials can be employed for this application, such as polymers, ceramics, and composite substances. Since natural bone is a complex inorganic-organic nanocomposite, the development of biomimetic composite biomaterials has emerged as an auspicious approach for bone tissue engineering applications [12,13]. Hydroxyalkanoates, derived from microorganisms, are promising materials due to their ability to form stable electroactive solutions and their ease of processing into nanofibers via electrospinning [14]. Moreover, they possess biocompatibility and biodegradability, making them even more attractive for use in biomedical applications [15]. Polyhydroxybutyrate (PHB) is particularly promising among polyhydroxyalkanoates (PHA) due to its specific properties and suitability for applications in bone tissue engineering [16]. Recent studies have demonstrated that PHB has superior mechanical properties when compared to other polymers for similar applications [17]. In addition, the modulus of elasticity of PHB is 0.14 GPa, which is within the range of natural bone (0.1–23.0 GPa) [18]. PHB possesses inherent piezoelectric properties [19,20] which are increasingly recognized for their significant role in promoting tissue regeneration and enhancing the healing and functional recovery of critical biological systems such as the heart, bones, and nervous tissues [21]. Also, PHB exhibits non-toxic and degradable properties, and its degradation products are biocompatible [22]. Some of these products, such as D-3-hydroxybutyrate, are present in the natural components of human blood plasma [23]. Furthermore, its gradual degradation aligns with the formation of new bone tissue. This ensures a temporary mechanical support until full regeneration is achieved. However, PHB mechanical performance and osteocompatibility are still limited, highlighting the need for further advancements in bone tissue engineering using these polymers. The combination of organic matrices and bioactive inorganic particles could be a promising candidate for biomedical applications [24,25].

Niobium pentoxide (Nb_2O_5) has been recognized as an excellent material for biomedical applications due to its biocompatibility and positive interactions with the human body [26]. Moreover, it can enhance cell adhesion, differentiation, and proliferation [27], facilitate the growth of hydroxyapatite crystals [28], and increase alkaline phosphatase activity [29]. Comparative studies on the biological performance of Nb_2O_5 have revealed significantly higher mitochondrial activity, cell proliferation, and in vivo osteointegration rate compared to titanium and stainless steel as implant materials [30,31].

A few reports exist on the preparation of composites based on PHB and niobium oxides. For instance, Heitmann *et al.* incorporated nanostructured niobium oxyhydroxide into PHB films to develop a recyclable photocatalytic material active under UV and visible light. FTIR-ATR and SEM analyses showed that the particles were uniformly dispersed and formed fine agglomerates within the PHB matrix [32]. In a subsequent study, the same authors investigated how different preparation methods influenced the morphology, nanoparticle dispersion, and thermal properties of PHB/niobium oxyhydroxide nanocomposites [33].

However, to the best of our knowledge, no detailed study has yet focused on the fabrication of electrospun PHB fibers containing niobium-based fillers. In this context, the present study aims to develop novel bioactive electrospun composite scaffolds based on PHB and Nb_2O_5 for bone tissue engineering applications. The incorporation of Nb_2O_5 is intended to enhance the mechanical properties of the membranes while imparting bioactivity. Scaffolds with different concentrations of Nb_2O_5 were investigated to comprehensively assess the effects of particles on the size, morphology, physico-mechanical, and thermal properties of the electrospun fibers. Additionally, a biological evaluation was conducted to evaluate the potential applications of these fibers in bone tissue engineering.

2. Experimental

2.1. Materials

Niobium oxide powder, kindly provided by Brazilian Company of Metallurgy and Mining- CBMM (Brazil), was used. PHB in powder form (Mw = 223 kDa, Tm = 175 0.3 °C, Mw/Mn = 1.23) was supplied by Biomer (Germany). N,N-dimethylformamide (DMF) was sourced from Aldrich used without further purification. Human Bone Marrow-Derived Mesenchymal Stem Cells (hBMSCs) were purchased from American Type Culture Collection (ATCC, Manassas, VA, USA) and cultured in complete growth medium (GM) α-Minimum Essential Medium (α-MEM) supplemented with 10 % (v/v) fetal bovine serum (Sigma-Aldrich, Milan, Italy), 100 U/mL of penicillin, and 100 μg/mL of streptomycin (Sigma-Aldrich) at 37 °C under a humidified 5 % CO_2 atmosphere. Filtered D-Phosphate Buffered Saline (PBS), (Euroclone) was used for niobium oxide release analysis.

2.2. Preparation and characterization of Nb_2O_5 particles

The average size of Nb_2O_5 particles was investigated by field emission scanning microscopy (SEM, QUANTA200, FEI, The Netherlands).

The powder was then treated in a PM 100 Planetary Ball Mill (Retsch GmbH, Haan, Germany) equipped with a 250 cm^3 zirconia jar loaded with 250 zirconia balls (0.5 cm in diameter) for 2 h at 400 rpm to obtain finer Nb_2O_5 particles. Dispersions of milled Nb_2O_5 particles (0.004 mg L−1) were prepared by sonication in DMF and in deionized water, using a Sonics Vibracell VC505 Ultrasonicator, for 50 min at 30 s intervals (amplitude of 20 %). Particle size distribution and zeta potential were determined by dynamic light scattering (DLS) using a Malvern® Zetasizer Nano instrument. All measurements were performed in triplicate.

2.3. Preparation of solutions for electrospinning

A 9 % (w/v) PHB solution in $CHCl_3$/DMF (9:1) was prepared. Specifically, PHB was dissolved in $CHCl_3$ at 55 °C for 1 h, after which DMF was incorporated into the solution at room temperature.

For the development of hybrid fibers, a Nb_2O_5 dispersion in DMF, obtained as described in Section 2.2, was added to the PHB solution and stirred for 30 min at room temperature. Different amounts of Nb_2O_5 particles (1, 3 and 6 wt% with respect to PHB) were incorporated into the PHB solution, resulting in the following code formulations: PHB, PHB-Nb1, PHB-Nb3, PHB-Nb6.

2.4. Electrospinning conditions

Each solution (3 mL) was placed in a syringe coupled with a 26-G stainless steel needle. The fibers were obtained using an NF 500 – Mecc Co equipment. Ltd setup. Each solution (3 mL) was placed in a syringe coupled with a 26-G stainless steel needle. The fibers were obtained using an NF 500 – Mecc Co equipment. Ltd setup. The fibers were

collected on a plate covered with an aluminum foil for 2 h using a voltage of 20 kV, feed rate of 0.5 mL/h, working distance of 30 cm (distance between the collector and the needle), relative humidity of ~37 % and ambient temperature (~25ºC).

2.5. Physico-chemical and mechanical characterization of membranes

2.5.1. Morphological analyses (SEM)

Morphological analyses of particles and fibers were performed by field emission scanning microscopy (SEM, QUANTA200, FEI, The Netherlands) with a 3.5 nm resolution at 30 kV (high vacuum). Before analysis, the samples were coated with a gold-palladium (Au–Pd) alloy using a Baltec Med 020 Sputter Coater System (Balzers AG, Balzers, Liechtenstein). The average fiber diameter distribution was determined using ImageJ software (National Institutes of Health, Bethesda, USA), based on micrographs taken from randomly selected areas (n = 40 fibers).

2.5.2. Contact angle measurements

The wettability of PHB/Nb_2O_5 fibers was evaluated using a Micro-Drop® (First Ten Angstroms Inc., Italy) contact angle meter associated with a high-speed framing camera. A drop of water (4 µl) was deposited on the surface of the fibers at room temperature by a syringe. The contact angle (θ) was determined using an FTA1000 Manual Drop Shape Analysis Software 2.0 version (FTA Inc. Portsmouth, Virginia, USA). It is defined as the angle between the investigated surface and the tangent from the edge of the water drop. Results represent the average values obtained from four measurements for each sample.

2.5.3. Fourier Transform Infrared Spectroscopy (FTIR-ATR)

FTIR-ATR spectra of neat and composite PHB-based fibers were acquired using the attenuated total reflection (ATR) mode, with a Thermo Fischer Scientific Nicolet 6700 equipped with a universal-ATR accessory. Spectral analysis was conducted under ambient conditions of room temperature and humidity. Each spectrum comprised 32 scans in the range region of 600–4000 cm^{-1} (resolution of 4 cm^{-1}).

2.5.4. Thermal analyses (DSC)

Thermal properties of fibers were evaluated by using TA DSC-Q2000 differential scanning calorimeter, equipped with a TA instrument DSC cooling system. Samples of 3 mg were heated from −20–250 °C at 10 °C min^{-1} and maintained at that temperature for 2 min; then, they were cooled to −20 °C at 10 °C min^{-1}. After a 2 min isothermal stage at −20 °C, the samples were reheated to 250 °C at the same rate. The process was conducted under a flow of nitrogen gas of 30 mL/min. The crystallinity degree (χ_c) of the prepared scaffolds was calculated by the following equation:

$$\chi_c \quad (\%) \quad = \quad \frac{\Delta H_m}{\Delta H_m^0} \times 100$$

Where ΔH_m is the heat of melting (J/g) and ΔH_m^0 is the heat of melting of 100 % crystalline PHB, which corresponds to 146 J/g [34]. The glass transition temperature was identified as the peak of the maximum obtained using the first derivative method.

2.5.5. Wide-Angle X-ray Diffraction (WAXD) analysis

Wide-angle X-ray diffraction (WAXD) patterns for electrospun PHB and its composites were obtained using a PANalytical PW3040/60 X'Pert PRO MPD diffractometer. The measurements were conducted in Bragg–Brentano geometry with the instrument operating at 45 kV and 40 mA. A high-power ceramic X-ray tube (model PW3373/10 LFF) equipped with a copper (Cu) anode served as the radiation source. Diffraction data were collected using Ni-filtered Cu Kα radiation (λ = 0.15418 nm), at a continuous scan rate of 0.04° per second over a 2θ range from 5° to 50°. The degree of crystallinity (χc) is the ratio of the total area under the resolved crystalline peaks to the total area under the unresolved X-ray scattering curve [35].

2.5.6. Tensile tests

Mechanical characterization of membranes was performed through tensile tests using an Instron 5564 test machine on rectangular-shaped specimens. An elongation rate of 5 mm/min was employed throughout the tests with a load cell of 100 N. The thickness of each sample was measured in three different locations using a digital micrometer. All tests were performed at ambient temperature. Seven specimens of each sample were tested, and average values were considered.

2.5.7. In vitro degradation studies

The hydrolytic degradation of membranes was evaluated by in vitro tests in phosphate-buffered saline (PBS) medium. Samples of around 10 mg (30 mm × 40 mm), immersed in 10 mL of PBS (pH 7.4) at 37 °C, were withdrawn and washed with distilled water at fixed times. After gently drying them with filter paper, they were carefully weighed for water uptake measurements (Eq. 1). Then, they were dried in a vacuum oven at room temperature for 72 h and weighed again to assess the weight loss (Eq. 2). All the experiments were performed in triplicate.

$$Weight\ loss(\%) = \frac{W_0 - W_{td}}{W_0} \times \quad 100 \tag{1}$$

$$Water\ uptake(\%) = \frac{W_{tw} - W_0}{W_0} \times \quad 100 \tag{2}$$

Where W_0 corresponds to the initial weight of dry samples, while W_{td} *and* W_{tw} represent the wet and dry weight at any given time, respectively.

SEM observation and DSC analysis were performed on dry samples at the end of the investigation period (120 days) of immersion.

2.5.8. Release of Nb ions

To determine the concentration of released Nb ions, PHB-Nb1, PHB-Nb3, and PHB-Nb6 membranes (1 cm×1 cm) were placed in PBS, and the release kinetics were performed at constant temperature (37 °C). The concentration of Nb ions was measured after every 24 h for 5 days of immersion using an inductively coupled plasma atomic spectrometer (Shimadzu ICPE-9800, Shimadzu Italy, Milan) configured with a water ignition mode and a mini torch. The spectrometer was operated at a radio frequency power of 1.20 kW with gas flow rates of 10.00 L/min for the plasma gas, 0.60 L/min for the auxiliary gas, and 0.70 L/min for the carrier gas. The exposure time was set to 30 s with an axial view direction. The emission lines of niobium measured were 309.418 nm, 316.340 nm, and 313.079 nm. For sample analysis, 1 mL of medium was diluted with 4 mL of HNO_3 7 %

2.6. Biological characterization

2.6.1. Cells culture

BMSCs were cultured in growth medium (GM) under standard conditions. For osteogenic differentiation, the cells were incubated in osteogenic induction medium (OIM), consisting of GM enriched with 100 nM dexamethasone, 10 mM β-glycerophosphate (Sigma-Aldrich), and 50 µg/mL ascorbic acid (Sigma-Aldrich). The medium was refreshed every three days.

2.6.2. Biocompatibility

Before cell seeding, the electrospun scaffolds were sterilized by 20 min of ultraviolet (UV) exposure and subsequently rinsed with PBS. The scaffolds were then positioned at the bottom of tissue culture plate wells, and cells were seeded onto them using growth medium (GM). Cell-scaffold interactions were evaluated by performing a CCK-8 assay, following the manufacturer's instructions. Lactate dehydrogenase

(LDH) released into the growth medium, as a consequence of cell membrane damage, was quantified according to the method described by Valentino *et al.* [36]. The capability of scaffolds to support cell adhesion was investigated using scanning electron microscopy (SEM, QUANTA200, FEI). After 14 days, cells were fixed with 2.5 % Glutaraldehyde for 1 h, washed twice with PBS for 30 min and then dehydrated through a graded series of ethanol, vacuum dried, mounted onto aluminum stubs, and ultimately sputter coated with gold.

2.6.3. Alkaline Phosphatase (ALP) Activity

To examine the osteogenic differentiation potential of the electrospun membrane, hBMSC cells were cultured in the presence of PHB, PHB-Nb1, PHB-Nb3, and PHB-Nb6 materials for 1, 7, 14, and 28 days in GM or OIM. ALP activity was determined as reported by Calarco *et al.* [37], testing hBMSC lysate with and without osteogenic induction. Data were normalized based on the total protein content of each sample. Each experiment was performed in quadruplicate and shown as the mean ± standard deviation (S.D.).

2.6.4. Alizarin red assay

Calcium precipitates within cells were detected through alizarin red staining. Cells (1 ×105/well) were seeded in a 12-well plate in the presence of electrospun membranes and cultured with or without osteogenic induction medium for 28 days. Then, cells were washed twice with PBS and fixed in 4 % formaldehyde in PBS for 15 min at room temperature (RT). Subsequently, cells were washed with water before being stained in 1 % Alizarin Red S solution (Sigma-Aldrich) for 30 min at room temperature with gentle shaking. The remaining dye was washed out through washes with tap water, and cells were observed under an optical microscope. Moreover, Alizarin Red staining was quantified by measuring the absorbance of the eluted stain at 550 nm using a spectrophotometer and normalizing it to the total protein content.

2.6.5. Expression of osteogenic-related genes (RT-PCR)

The multipotent nature and differentiation potential of hBMSCs were validated using reverse transcription-polymerase chain reaction (RT-PCR). For osteogenic differentiation, cells were cultured at 5 × 103 cells/well in 6-well plates until 50 % confluence. Then the GM was replaced with OIM and/or PHB-Nb1, 3, and 6 as described previously. The cultures were maintained for 3 weeks before Real-time PCR analysis. Total RNA was extracted from cell cultures using TriFast reagent (EuroClone, Milan, Italy) according to the manufacturer's protocol. The synthesized cDNA was used as a template to evaluate the target genes using specific primers: *type I collagen* (*ColIA1*), *transcription factor Sp7, also called osterix* (*OSX*), *alkaline phosphatase* (*ALP*), *runt-related transcription factor 2* (*RUNX2*), *osteopontin* (*OPN*), and *osteocalcin* (*OCN*). *Glyceraldehyde-3-phosphate dehydrogenase* (*GAPDH*) gene was considered the housekeeping gene used for normalization. Table 1 shows the primer sequences used. Relative markers expression ratio was calculated based on the comparative threshold cycle C_t method ($2^{\Delta\Delta CT}$). All reactions were run in triplicate and were normalized to the housekeeping genes.

2.6.6. Statistical analysis

Statistical analyses were performed using GraphPad Prism software, version 8 (GraphPad Software, San Diego, CA, USA). Data are presented as mean ± standard deviation (S.D.). One-way ANOVA followed by Tukey's post hoc test was used to assess statistical significance, which was defined as $p < 0.05$. Results are based on three independent experiments, each carried out in at least duplicate.

3. Results and discussion

3.1. Nb_2O_5 particles

The average diameter of Nb_2O_5 particles was preliminarily evaluated through SEM analysis, and the size distribution was determined by using Image J (Figure S1). The particles exhibited an average size of 44 μm. They were then treated by ball milling, and the obtained size distribution was investigated using DLS. Ball milling is a widely used method for reducing particle size. However, parameters such as milling duration and solvent presence can significantly impact the final particle dimensions. Typically, this process yields particles smaller than 200 nm, which may tend to form stable agglomerates or adhere to larger particles [38]. To separate these coarse particles, they were dispersed in DMF and subjected to sonication. DLS analyses were performed immediately after sonication to prevent sedimentation [39] and to evaluate both particle size and zeta potential. A size distribution centered at 657.0 ± 0.3 nm was observed, indicating that sub-micron particles were successfully obtained through the ball milling process. Additionally, an average zeta potential of −42 mV was measured. This value is consistent with the literature and confirms the formation of a stable colloidal dispersion of the solids in the suspension [40].

3.2. Preparation of electrospun PHB-based fibers

Several electrospinning conditions were tested to optimize the production of PHB-based fibers. Different voltages, spinning distances, and feed rates were investigated to form a stable Taylor cone and solution jet, thereby obtaining uniform and continuous fibers. It was observed that by applying a voltage of 20 kV, at a 30 cm distance between collector and spinneret and using a feed rate of 0,5 mL/h, nearly bead-free, randomly oriented PHB-based fibers with different Nb_2O_5 content were successfully produced. The values of voltage, flow rate, and spinneret-collector distance were kept constant for all the experiments.

3.2.1. Morphological analysis (SEM)

The influence of Nb_2O_5 on the fiber morphology was studied by SEM (Fig. 1). Neat PHB fibers exhibited a relatively homogeneous surface and uniform size along the fiber axis, except for the presence of some ellipsoid or spherical polymer grains, with an average diameter of 1.010 ± 0.105 μm. As reported in literature, the slight nonuniformity can be attributed to the low conductivity of the PHB solution that, in its turn, affects the solution jet during the process and therefore the fiber morphology [41]. The presence of niobium pentoxide at 1 and 3 wt% affected the fiber size, reducing their diameters by approximately 16 %, likely due to the effect of particles on the solution conductivity. N_2O_5 is well recognized for its outstanding electronic properties and has been

Table 1
Primers used for qRT-PCR.

Gene	Accession number	Forward Primer (5′–3′)	Reverse Primer (5′–3′)
RUNX2	NM_001015051.4	AGCCAGGTTCAACGATCTGA	TAGCTCTGTGGTAAGTGGCC
ALP	NM_000478.6	CAGATGCCAACTTCCCACAC	GGTCCCCTTTCTTGCAGTTG
Sp7/OSX	NM_152860.2	CCCTCCCTTTTCCCACTCAT	TGGGCAGACAGTCAGAAGAG
COL1A1	NM_001173467.3	TAAGTCCCTTTCTGCCCGTT	ATTTGGGAAGGAGTGGAGGG
OCN	NM_000088.4	GCGCTACCTGTATCAATGGC	AACTCGTCACAGTCCGGATT
OPN	NM_000582.3	TTTCACTCCAGTTGTCCCCA	GGATGTCAGGTCTGCGAAAC
GAPDH	NM_001256799.3	TAGCGGCTAGCGGTAT	CGGGGCTATGGCTAGCTAGCTTTC

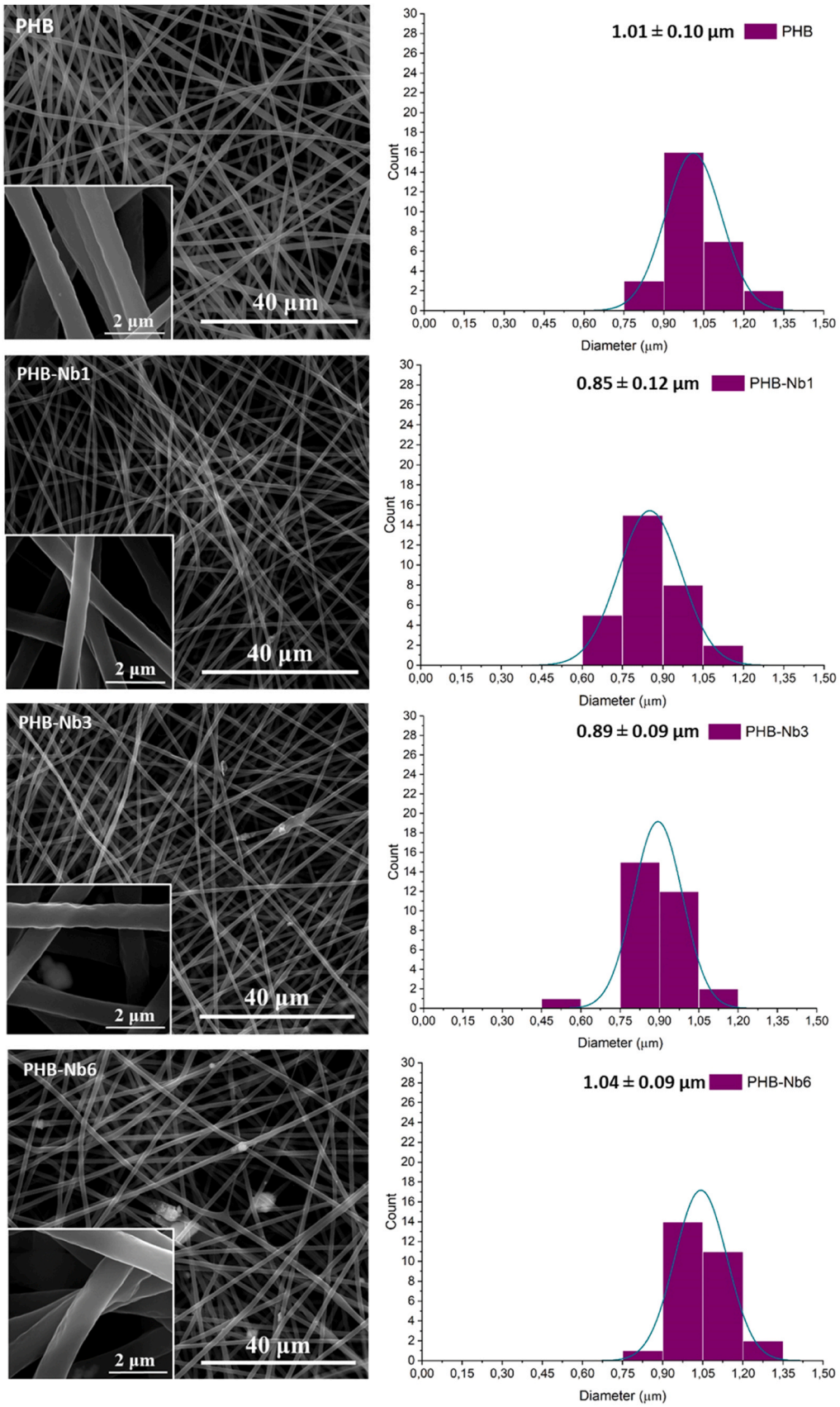

Fig. 1. SEM micrographs along with histograms showing the size distribution of PHB, PHB-Nb1, PHB-Nb3, PHB-Nb6 fibers, calculated by ImageJ software (fiber number = 40).

extensively utilized in both microelectronic and optoelectronic applications [42,43]. Therefore, the presence of a low amount of Nb_2O_5 slightly alters the morphology of the fibers by enhancing solution conductivity, leading to more homogeneous and nearly defect-free fibers compared to the PHB ones. As reported in literature [44], particles dispersed in DMF are more concentrated in the fiber core because of the highest boiling point of DMF. During the electrospinning process, CF evaporates immediately, and DMF is concentrated in the bulk, where most of the particles remain [45]. However, by increasing Nb_2O_5 concentration up to 6 wt%, the overall effect of particles on fiber morphology was completely different: a rough surface and some irregularities in the fiber shape were noticeable, and the average diameter is similar to that of the PHB fibers. This evidence suggested that the effect of increased conductivity was counteracted by the higher amount of Nb_2O_5 particles, which tend to agglomerate into larger clusters, despite the rigorous sonication procedures used in this work, resulting in rougher fiber surfaces and reduced uniformity [46].

3.2.2. Water Contact Angle (WCA)

Contact angle measurements of electrospun fibrous mats are crucial for tissue engineering applications, as they provide insight into surface wettability and hydrophilicity. These properties significantly impact cell adhesion, proliferation, and differentiation, processes that are essential for tissue development and integration. Plain PHB fibers exhibited a contact angle of $126.5 \pm 0.6°$, according to a very hydrophobic surface. Notably, the addition of Nb_2O_5 particles did not significantly affect WCA which remained at $126.8 \pm 0.4°$, $128.3 \pm 0.2°$ and $126.9 \pm 1.1°$ for PHB-Nb1, PHB-Nb3 and PHB-Nb6, respectively. This result suggested that the inorganic particles were likely either embedded within the fibers or present at the surface in amounts insufficient to affect surface wettability of hybrid fibers, as initially suggested by SEM analysis [47].

3.2.3. FTIR-ATR analysis

Fig. 2a and b show the FTIR-ATR spectra of pure PHB and PHB/Nb_2O_5 electrospun membranes.

The PHB spectrum showed bands between 3100 and 2900 cm^{-1} relative to the symmetrical stretching of the CH_3 group, along with bands from 1460 to 1380 cm^{-1} associated with asymmetric stretching of CH_3 and CH_2 groups. Moreover, in the region between 1300–1100 cm^{-1} bands relative to C-O-C in both crystalline (i.e., 1274 and 1226 cm^{-1}) and amorphous (i.e., 1261 and 1180 cm^{-1}) phases were detected. Peaks appearing in the range 1700–1650 cm^{-1} are related to carbonyl stretching vibrations of PHB ester groups [32]. In particular, two major C═O stretching bands were detected at 1746 and 1720 cm^{-1}, corresponding to the amorphous and crystalline states, respectively [48]. This evidence suggested a semicrystalline nature of the electrospun fibers. The spectra of PHB/Nb_2O_5 with different niobium oxide content exhibited a comparable band pattern. Unfortunately, the presence of Nb_2O_5 particles could not be detected since most of its typical vibration frequencies (e.g., 640 cm^{-1} ascribed to the symmetric stretching of Nb-O-Nb, and the shoulder peak at 853 cm^{-1}, corresponding to the asymmetric stretching of Nb═O, are masked by signals related to PHB [48]. A deconvolution of PHB bands in the carbonyl region was performed for all the samples to assess the effect of inorganic particle presence on their position and shape (Figure S2). Indeed, these groups play a crucial role in the organization of polymer crystals, and their corresponding signals are often used to investigate the intramolecular and intermolecular interactions they are involved in [49]. Figs. 2c and

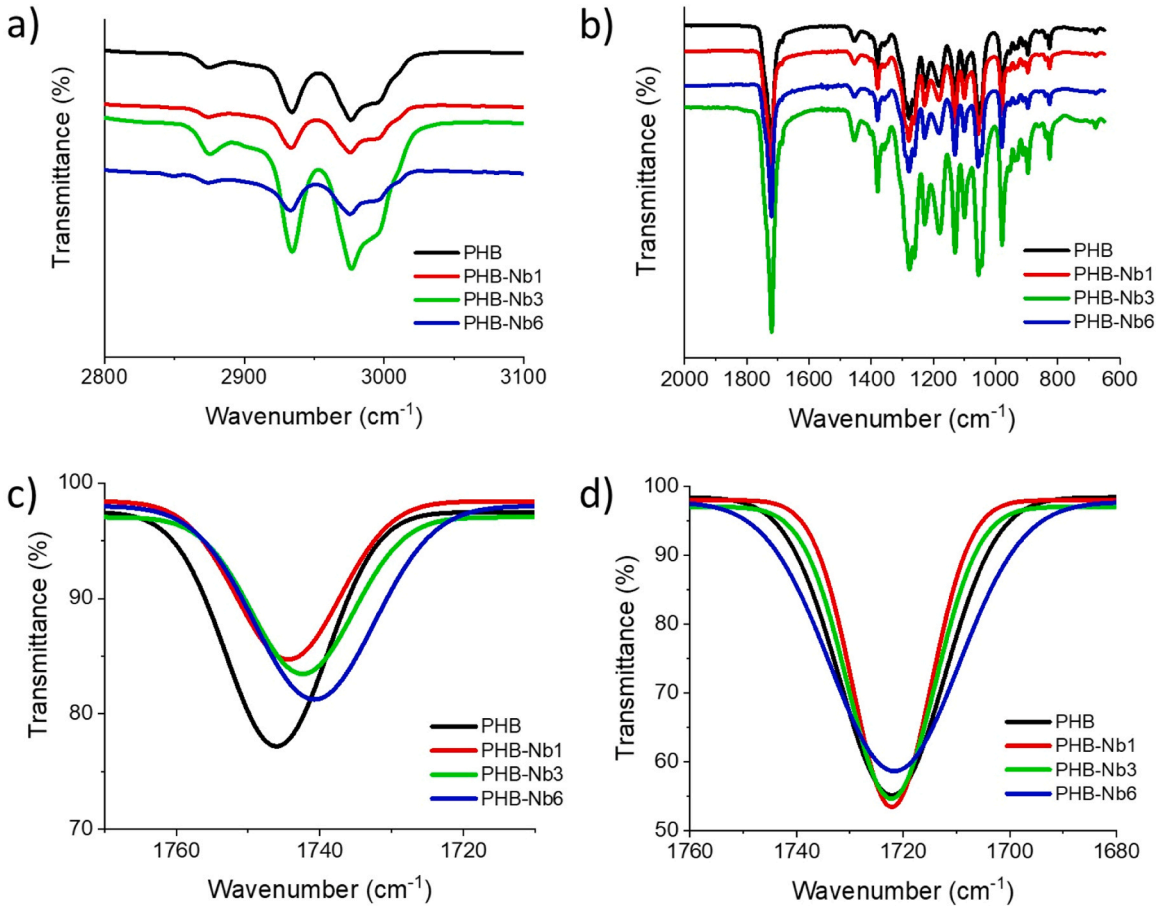

Fig. 2. FTIR-ATR analysis of neat and composite PHB-based fibers: spectra in the region between 3100 and 2800 cm^{-1}(a), and in the region between 2000 and 600 cm^{-1} (b); deconvoluted bands at 1740 cm^{-1} (c) and 1720 cm^{-1} (d).

2d show an overlapping of deconvoluted peaks at 1746 cm^{-1} (C═O amorphous) and 1720 cm^{-1} (C═O crystalline) for PHB and its composites, respectively. The relative intensity of amorphous and crystalline C═O bands suggested that all the samples were predominantly composed of a crystalline structure, with only a minor amorphous component. In addition, comparing these peaks across different formulations, it was possible to observe a smooth enlargement and a slight shift to lower wavenumbers of the band at 1746 cm^{-1} in the presence of increasing niobium concentration, reaching 1740 cm^{-1} in the case of PHB-Nb6. In contrast, any significant shift was detected for the peak around 1720 cm^{-1}. The vibrational frequency of a functional group is primarily influenced by the force constant and the mass of the atoms involved. Any interaction with these groups can modify their electron distribution, which in turn reduces the force constant and causes the peak to shift to lower frequencies. Therefore, this evidence suggested that physical interactions between the inorganic filler and the polymer matrix primarily involve the amorphous phase of PHB, which, being less ordered and stable, is more susceptible to interactions with niobium oxide [50].

3.2.4. Thermal analysis (DSC)

The DSC thermograms of the heating run of pure PHB and PHB-Nb systems are reported in Fig. 3a and b, respectively. The thermal parameters are collected in Table 2. A single melting peak was evident for all the samples in the region between 172 and 176 °C. In particular, PHB scaffold presented T_m picked at 175.0 °C. The melting temperature of the PHB/Nb_2O_5 composites did not undergo any changes, indicating that their crystal size remained similar to that of pristine PHB.

The crystallinity degree (χ_c) for PHB was 69.9 %, the incorporation of 1, 3 and 6 wt% of Nb_2O_5 in the PHB matrix decreased χ_c of 1, 5 and 10 %, indicating inhibition in the formation of stable nuclei for consolidation and growth of the crystallites. The addition of various fillers to the polymer matrix can result in either an increase or a reduction in the polymer's crystallinity [27,51]. Ho *et al.* demonstrated that the incorporation of 1 and 5 wt% of magnetite particles reduces the PHB and PHBV crystallinity of about 7 and 14 %, respectively, attributing this behaviour to physical hinderance of the filler to the proper arrangement of polymer chains [52].

As seen in Table 2, the T_g increased with the increase of Nb_2O_5 amount as a consequence of the reduced mobility of the macromolecular chains. DSC results confirmed physical interactions between the inorganic filler and the amorphous phase of PHB, as suggested by FTIR-ATR analysis.

Table 2
Thermal properties of PHB-based membranes before and after 4 months of immersion in PBS at 37 °C. Evaluation was performed in the first heating run.

Sample	Before immersion				After immersion		
	T_g (°C)	T_m (°C)	ΔH_m (J/g)	χ_c (%)	T_m (°C)	ΔH_m (J/g)	χ_c (%)
PHB	56.8	175.0	101.5	69.9	175.6	105.7	72.4
PHB-Nb1	57.4	174.6	101.4	69.4	174.2	110.4	73.2
PHB-Nb3	58.3	175.5	97.0	66.4	175.4	102.3	70.1
PHB-Nb6	58.8	174.9	91.8	62.9	174.4	101.2	69.3

3.2.5. WAXD analysis

Poly(3-hydroxybutyrate) (PHB) can crystallize into two distinct forms: the α-form and the β-form. The α-form typically forms when PHB is cooled from the melt and features an orthorhombic unit cell structure with a 3_1 helical chain conformation [52]. In contrast, the β-form emerges when tensile stress is applied to the oriented α-form, resulting in polymer chains adopting an almost planar zigzag arrangement. However, the exact crystal structure of the β-form remains unclear [53]. It is also important to note that the transition between these forms is not complete; even under strong tension, both α- and β-forms are present up to the point of material failure [54]

X-ray diffraction patterns of electrospun PHB (Fig. 4) show peaks consistent with those found in the literature [55], corresponding to the

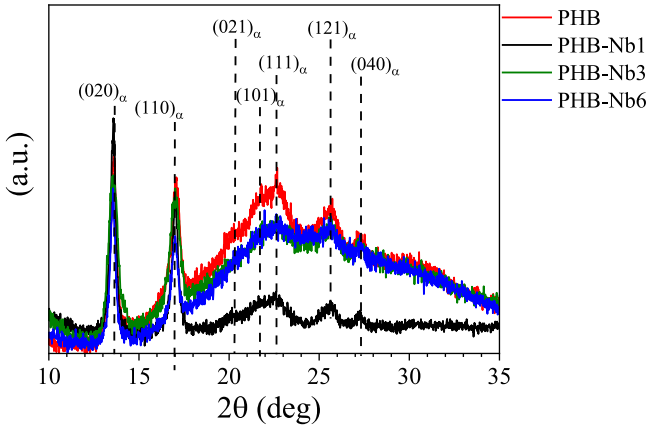

Fig. 4. Wide angle X-ray diffractograms for PHB and PHB/Nb_2O_5 composites.

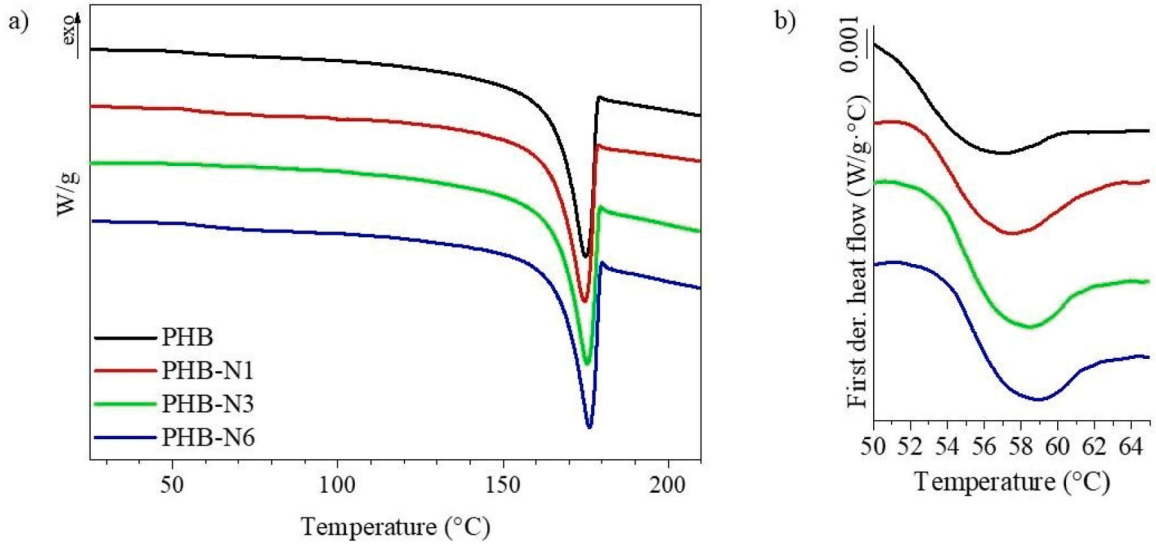

Fig. 3. DSC thermograms for pure PHB and PHB/Nb_2O_5 electrospun scaffolds. (a) First heating run; (b) First derivative of thermogram for T_g determination.

(020), (110), (021), (101), (111), (121), and (040) planes of the α-phase crystal lattice [56]. Incorporating Nb_2O_5 into the PHB matrix did not alter the unit cell structure but did reduce the material's degree of crystallinity. This is evidenced by the presence of an amorphous halo in all the composite samples. Specifically, the crystallinity index of pure PHB was 62 %, which dropped to 49 % in the PHB/Nb1 sample and further declined to 35 % in both PHB/Nb3 and PHB/Nb6 composites, also in agreement with the trend found by DSC measurements. Similar results were found by adding to PHB sugarcane bagasse fibers and cellulose nanofibrils [57,58].

3.2.6. Mechanical properties

Table 3 reports the Young's modulus, the tensile strength and the elongation at break of electrospun PHB and PHB/Nb_2O_5 composites.

The addition of Nb_2O_5 significantly affected the mechanical properties of electrospun PHB mats. Tensile strength progressively increased with a higher filler percentage. The highest tensile strength was observed when at 6 wt% Nb_2O_5, with two-fold increase compared to PHB fibers. Similarly, the Young's modulus increased with filler content reaching 85.50 ± 0.15 MPa for PHB-Nb6 which is approximatively three times the value observed for the pure PHB. Majerczak et al. [59] reviewed PHB composites with a wide variety of fillers to find trends between the filler type, crystallinity and mechanical properties. The data obtained from the literature do not provide conclusions about the effect of the degree of crystallinity on the tensile properties of PHB–filler composites. In fact, the mechanical properties are influenced by the fraction of amorphous and crystalline phases, but also by the interfacial regions, the nature of the filler, and the microstructure. The observed enhancement in tensile strength and Young's modulus, despite the reduced crystallinity, can likely be attributed to the reinforcing effect of Nb_2O_5 particles. These particles act as rigid fillers and, through adequate interfacial adhesion with polymer matrix, enhance stress transfer, thereby compensating for the loss of crystalline domains [60,61]. Interestingly, the increase in modulus was more pronounced at higher filler concentration, probably due to the effect of particles agglomeration [62]. At 3 and 6 wt% of Nb_2O_5, agglomerates become more prevalent and contribute significantly to the material stiffness. Finally, the elongation at break increased across all compositions. This behavior may be related to the failure mechanism, which involves particle-matrix debonding and the formation of large voids that coalesce during matrix fibrillation, as reported in literature [63].

3.3. Hydrolytic degradation

The hydrolytic degradation of the membranes was evaluated by soaking samples in PBS (pH 7.4) at 37 °C. After 120 days, membranes (which could still be handled) were withdrawn, washed with distilled water, and dried for both SEM observation and DSC analysis.

Fig. 5a shows SEM micrographs of scaffolds along with the size distribution of fibers. All the samples retained the original fibrous morphology with no significant changes detected on their surfaces, which remained homogeneous and smooth. No disintegration of individual filament or short segment was noticeable. This evidence indicated that the neutral pH used in the study did not accelerate the degradation of fibers, which proceeds slowly under these conditions and takes longer than the investigation period [64]. Only neat PHB exhibited a slight decrease in the average fiber size, from 1.010 ± 0.105 μm to 0.753 ± 0.091 μm following the immersion in PBS, while a slight increase was observed for the hybrid fibres. Even if it is often reported that the increased amorphous content in PHB accelerates its degradation, many other factors affect the degradation kinetics in the case of polymer-composites scaffolds [65]. The presence of filler, for example, can influence the autocatalysis process, often associated with scaffolds produced from aliphatic polyesters, water uptake (as found in our work), and diffusion, thus counteracting PHB acidic degradation. This finding suggests a weak influence of the filler on hydrolytic degradation in the early stage of degradation (i.e., 120 days).

During the degradation period, samples were weighed at prefixed times, both in the dry and wet states, to monitor weight loss and water uptake, respectively. In addition, the pH of the degradation medium was measured at the beginning and at the end of the investigation period. The weight of the dry samples showed no significant variation during the investigation period. Only a decrease of around 2 % was observed for all the analyzed samples. Fig. 5b shows the water uptake as a function of immersion time. In the first 20 days, no significant weight variation was detected. After that time, a weight increase was observed for all the samples till a plateau was reached, with PHB showing the highest water uptake ability. Although composite fibers typically have lower crystallinity and theoretically greater swelling ability than pure PHB membranes, the particles embedded within the polymer matrix may hinder PBS from penetrating the polymer network, thereby reducing swelling and slowing hydrolytic degradation [27,66]. The pH was measured, and it remained constant along the whole degradation assay, around 7.4 [29]. Although the degradation of PHB ultimately produces the biocompatible 3-hydroxybutyric acid, the very slow degradation probably prevented the release of low-molecular-weight acidic compounds that could have altered the pH of the medium [67].

The thermal properties of the membranes after 120 days of soaking in PBS were assessed using DSC and compared to those of freshly prepared scaffolds, as shown in Table 2. PHB exhibited a semicrystalline behaviour across all samples, even after immersion in PBS. The melting temperature remained unchanged during the entire immersion time, while all samples showed a slight increase in ΔH_m, resulting in a modest rise in crystallinity. The small increase in crystallinity is likely due to a slight selective degradation of the amorphous fraction, which leads to a partial reorganization of the polymer chains in the crystalline regions. However, these results indicated that the microstructure of PHB scaffolds remained largely unaffected during the investigated period [64].

Table 3
Mechanical properties of PHB electrospun membranes without or with different concentrations of Nb_2O_5.

	Young's modulus (MPa)	Tensile strength at break (MPa)	Elongation at break (%)
PHB	32.71 ± 0.02	1.5 ± 0.1	50.9 ± 19.1
PHB-Nb1	33.83 ± 0.08	2.0 ± 0.3	66.3 ± 28.2
PHB-Nb3	45.92 ± 0.03	2.3 ± 0.1	63.7 ± 7.2
PHB-Nb6	85.50 ± 0.15	3.3 ± 0.3	93.1 ± 13.6

3.4. Biocompatibility and Nb ions release

Before designing a new biomaterial for tissue engineering, it is crucial to ensure that it poses no risk when implanted in the body. Therefore, in vitro biocompatibility tests and cell morphology analysis were performed to assess the ability of PHB/Nb_2O_5 to interact safely and effectively with biological systems. As shown in Fig. 6a, CCK-8 assay demonstrated that Nb ions concentration did not affect hBMSCs metabolic activity at all time points. In addition, the low LDH level in the cell supernatant confirmed the absence of cell membrane damage (Fig. 6b). Morphological analyses of cells cultured on electrospun scaffolds show that hBMSCs are able to colonize and adhere to all the substrates, adopting a spreading morphology, indicative of robust attachment (Figure S3). Cell filopodia extending along the fibers could be observed on all types of nanofibrous scaffolds. These findings align with previous studies indicating that niobium exhibits lower cytotoxicity, both in vitro and in vivo, compared to other metal ions [68,69].

The release of Nb ions was measured to evaluate the potential of electrospun membranes in promoting an osteogenic phenotype in

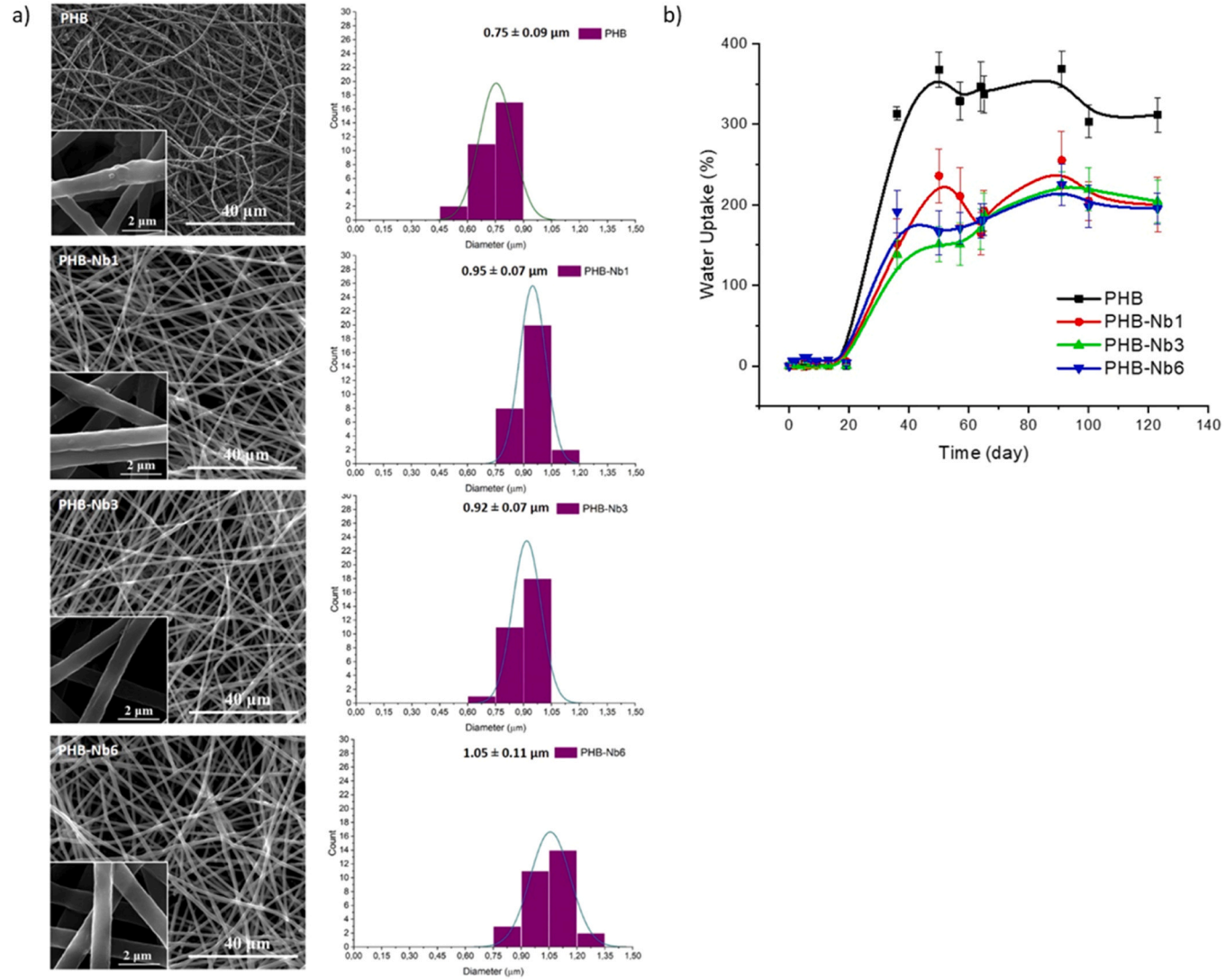

Fig. 5. (a) SEM micrographs along with histograms showing the size distribution of PHB, PHB-Nb1, PHB-Nb3, PHB-Nb6 fibers after soaking in water. (b) Water uptake (%) curves for pure PHB and PHB/Nb2O5 composite electrospun fibers as a function of immersion time.

mesenchymal stem cells, including their ability to support mineralization and alkaline phosphatase activity. As shown in Fig. 6c, the concentration of Nb ions released at 37 °C increased during the immersion period for all analyzed samples. As expected, Nb ion concentration released from PHB-Nb6 was higher than that for PHB-Nb1 and PHB-Nb3 at each time point. In particular, the Nb ion concentration in the medium after 5 days of immersion was $5.39 \pm 0.21 \times 10^{-6}$ mol L^{-1} for PHB-Nb1, $7.38 \pm 0.29 \times 10^{-6}$ mol L^{-1} for PHB-Nb3, and $9.98 \pm 0.32 \times 10^{-6}$ mol L^{-1} for PHB-Nb6. Since the biodegradation of PHB is much slower than the timescale of the experiment, it can be assumed that only the Nb located closer to the surface of the fibers was rapidly released. Obata *et al.* demonstrated that the bioactivity of Nb_2O_5 was related to the Nb ion concentration present in culture medium [70]. Indeed, ALP activity was higher in cells cultured in medium containing 3×10^{-7} M Nb with respect to Nb-containing media or standard medium, regardless of whether the medium was supplemented with osteogenic factors. Similar trends were reported for yttrium, silicon, and zinc ions [71–73].

3.5. Osteoinductive potential

The incorporation of Nb_2O_5 into biomaterials has been explored for its ability to stimulate osteogenic cell functions and promote bone tissue regeneration, both in vitro and in vivo [59].

In this context, the osteogenic capability and molecular mechanisms of the PHB-Nb membranes were assessed using ALP activity, alizarin red staining, and qRT-PCR analyses. As shown in Fig. 7a, alizarin red staining on day 21 revealed that hBMSCs cultured in the presence of electrospun fibers exhibited larger calcified nodules with respect to the control, inducing mineralization of the matrix. As expected, calcium deposits increased in a concentration-dependent manner, with the higher mineralization in the presence of PHB-Nb6 membrane. Quantitative results supported the microscopic findings (Fig. 7b).

Consistently, the ALP activity of hBMCS cells cultured on Nb-containing membranes increases with increasing Nb_2O_5 content compared to those cultured in GM (CTL group), albeit in the absence of osteogenic supplementation. (Fig. 7c). ALP is a widely accepted early indicator of osteogenic differentiation; therefore, elevated ALP activity suggests that mesenchymal cells are progressing toward an osteogenic lineage.

Cells cultured in the presence of OIM were used as a positive control. b) Quantification of Alizarin red staining. The result was the representative of three different experiments. Statistically significant variations # $p < 0.05$, ## $p < 0.01$, and ### $p < 0.001$ *versus* CTL. c) Semi-quantitative analysis of ALP activity of cells cultured in the presence of Nb-containing membranes at days 1, 7, 14, 21, and 28. PHB was used as a negative control. The result was representative of three different

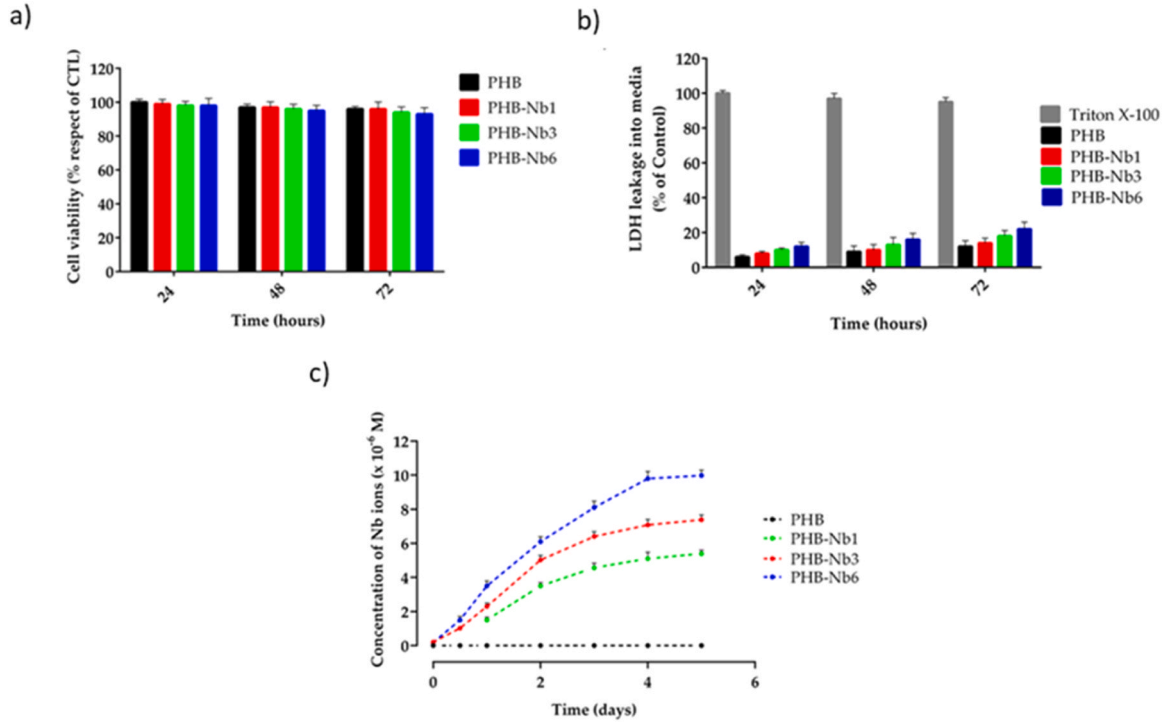

Fig. 6. Biocompatibility of PHB-based membranes tested via CCK-8 (a) and LDH (**b**) assays after 24, 48, and 72 h of incubation. (c) Nb ion concentrations after immersion for 1, 2, 3, 4, and 5 days in the growth medium (GM). For each sample, six different experiments were conducted, and the results were expressed as the mean of the values obtained (mean ± SD).

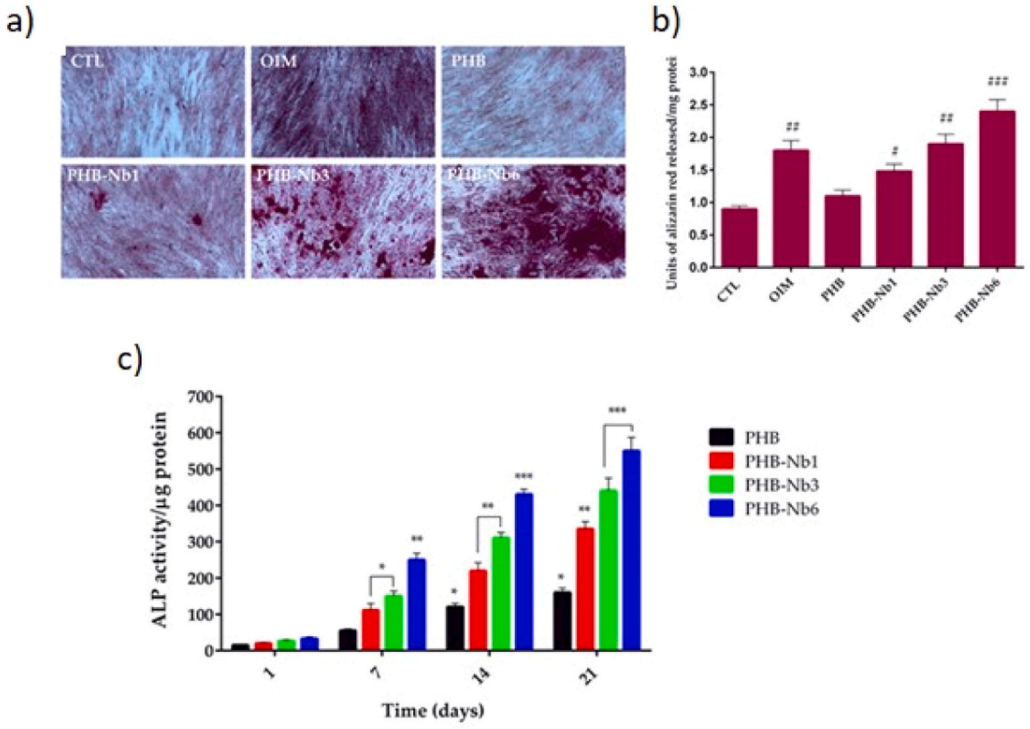

Fig. 7. Effects of niobium pentoxide on hBMSCs mineralization and ALP activity analysis. (a) Representative pictures of alizarin red S-stained assessed with transmitted light microscopy at 20X magnification of mineral nodules formed after 28 days of culture. Cells cultured in presence of OIM was used as positive control. b) Quantification of Alizarin red staining. The result was the representative of three different experiments. Statistically significant variations # $p < 0.05$, ## $p < 0.01$, and ### $p < 0.001$ versus CTL. c) Semiquantitative analysis of ALP activity of cells cultured in presence of Nb-containing membranes at days 1, 7, 14, 21, and 28. PHB was used as negative control. The result was representative of three different experiments. Statistically significant variations * $p < 0.05$, **$p < 0.01$ and *** $p < 0.001$ versus PHB.

experiments. Statistically significant variations * $p < 0.05$, ** $p < 0.01$ and *** $p < 0.001$ *versus* PHB. qRT-PCR analysis was carried out to evaluate the impact of Nb-containing fibers on genes associated with the osteogenic differentiation of mesenchymal stem cells (Fig. 8). In comparison with the CTL group, hBMSCs grown in the presence of PHB-Nb membranes showed an upregulated expression of all osteogenic differentiation-related genes examined for 21 days. In particular, the expression level by the cells cultured on PHB-Nb6 and PHB-Nb3 is comparable to that of cells cultured in the presence of OIM.

The obtained results are in line with those reported in the literature. Tan *et al.*[74] demonstrated an outstanding bioactivity of niobium in vitro, which is able to promote MC3T3-E1 cell adhesion, proliferation, and osteogenic differentiation without negatively affecting cell viability. Moreover, their study indicated that Nb implants could accelerate fracture healing more effectively than Ti6Al4V implants, as shown in a rat femur fracture model. The authors also found that the osteogenic effects of Nb were mediated through the activation of the PIK/Akt3 signaling pathway.

Marins *et al.* produced poly(lactic acid) nanofibers incorporated with niobium pentoxide nanoparticles, showing that the resulting

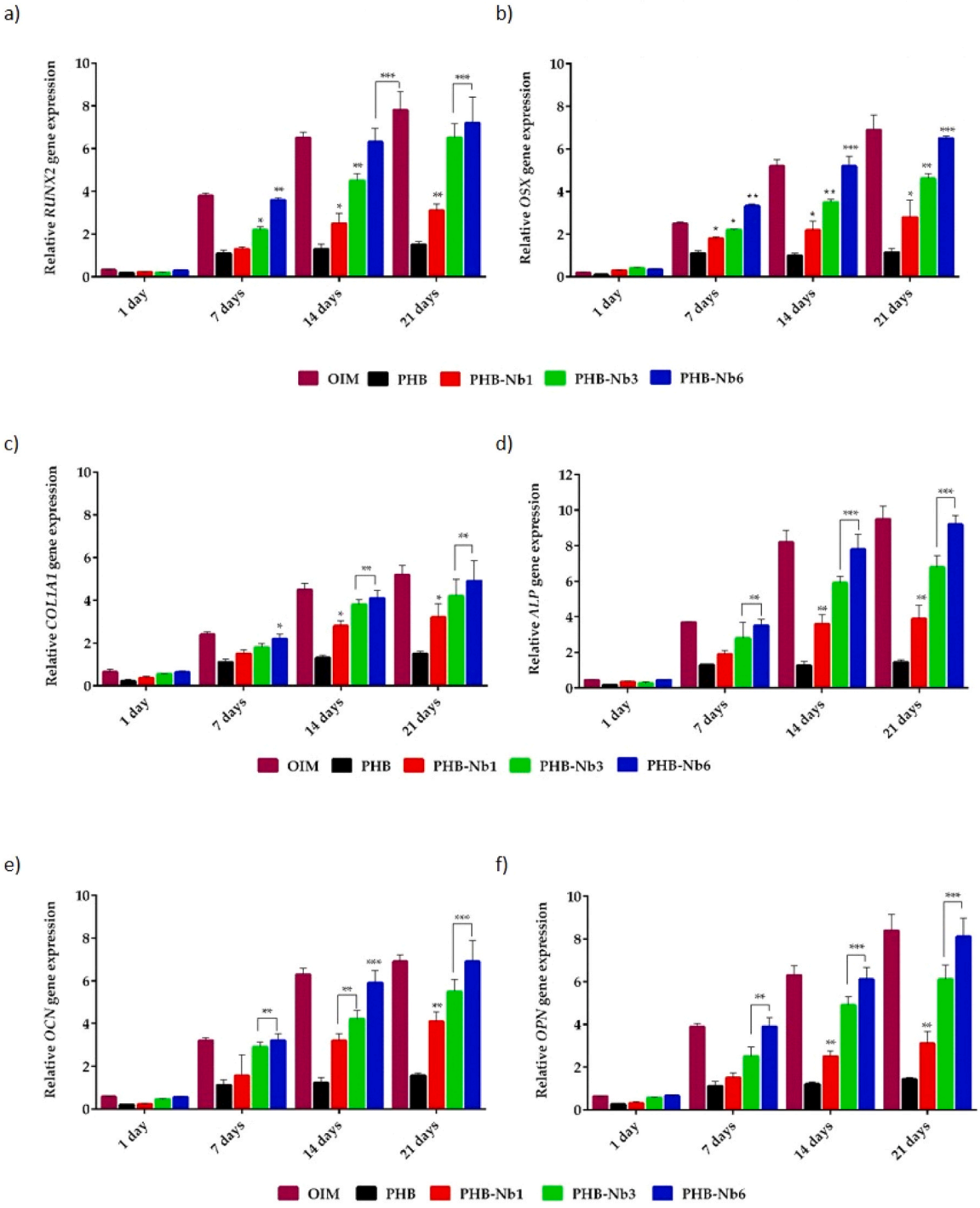

Fig. 8. Impact of Nb ions on the gene expression levels of a) *RUNX2*, b) *OSX*, c) *COL1A1*, d) *ALP*, e) *OCN* , and f) *OPN* in hBMSC cells for 21 days. Cells cultured in presence of OIM were used as positive control. *GAPDH* is used as housekeeping gene. Data represent the mean ± SD of three replicate experiments. Statistically significant variations * $p < 0.05$, ** $p < 0.01$ and *** $p < 0.001$ *versus* PHB.

membranes effectively enhance cell proliferation without compromising the wettability, porosity, or mechanical properties of the membranes [75].

In a separate study, the same authors developed composite membranes composed of polycaprolactone-gelatin-hydroxyapatite with varying concentrations of niobium pentoxide particles (PGHANb). Cell metabolism assays confirmed that the niobium-infused membranes were non-toxic and promoted cell proliferation and differentiation more effectively than the controls, highlighting their potential for bone tissue engineering applications.

4. Conclusions

In this work, composite fibers based on polyhydroxy butyrate and different amounts of niobium oxide were successfully prepared by electrospinning, and the effect of various concentrations of Nb_2O_5 on physico-chemical and biological properties was investigated. The electrospinning process was optimized to produce nearly bead-free, randomly oriented fibers. The influence of Nb_2O_5 on the fiber morphology was investigated using SEM, highlighting that the presence of niobium significantly reduced the diameters of the fibers, probably due to the effect of inorganic particles on the solution conductivity. By measuring the water contact angle, it was demonstrated that the filler did not affect membrane wettability, suggesting that the particles were embedded within the polymer matrix. FTIR-ATR analysis indicated the presence of physical interactions between Nb_2O_5 and PHB, primarily affecting its amorphous phase. Additionally, increasing Nb_2O_5 content reduced PHB crystallinity while significantly improving its mechanical properties. Notably, the Young's modulus for PHB-Nb6 reached 85.50 $\pm$ 0.15 MPa, three times higher than that of pure PHB. The hydrolytic degradation study showed that the presence of niobium oxide slightly slowed the degradation rate of the membranes in the early stages, as PHB degradation occurs over a much longer period than the duration of the study. Biocompatibility tests on hBMSCs confirmed the non-toxicity of all samples. Nb-containing membranes exhibited osteoinductive potential, as demonstrated by alizarin red staining and ALP assays, which revealed concentration-dependent increases in mineralization and ALP activity, with the highest levels observed for PHB-Nb6. Additionally, qRT-PCR analysis revealed upregulated expression of osteogenic differentiation-related genes in hBMSCs cultured with PHB/Nb_2O_5 membranes.

CRediT authorship contribution statement

Giovanna Gomez d'Ayala: Writing – original draft, Supervision, Funding acquisition. **Irene Bonadies:** Writing – original draft, Methodology, Investigation. **Yeda Bastos de Medeiros:** Writing – review & editing, Supervision, Funding acquisition. **Donatella Duraccio:** Writing – original draft, Methodology. **Anna Calarco:** Writing – original draft, Supervision, Data curation. **Anna Valentino:** Methodology, Investigation, Conceptualization. **Anna Raffaela de Matos Costa:** Methodology, Investigation, Data curation.

Declaration of Competing Interest

The authors declare that they have no known competing financial interests or personal relationships that could have appeared to influence the work reported in this paper.

Acknowledgments

The authors acknowledge the National Council for Scientific and Technological Development (CNPq), Brazil, for supporting the mobility of Dr de Matos Costa.

Appendix A. Supporting information

Supplementary data associated with this article can be found in the online version at doi:10.1016/j.mtcomm.2025.114177.

Data Availability

Data will be made available on request.

References

[1] A. Khodabandeh, A.A. Yousefi, S. Jafarzadeh-Holagh, E. Vasheghani-Farahani, Fabrication of 3D microfibrous composite polycaprolactone/hydroxyapatite scaffolds loaded with piezoelectric poly (lactic acid) nanofibers by sequential near-field and conventional electrospinning for bone tissue engineering, Biomater. Adv. 166 (2025) 214053, https://doi.org/10.1016/j.bioadv.2024.214053.
[2] N. Zhu, M. Ye, D. Shi, M. Chen, Reactive compatibilization of biodegradable poly (butylene succinate)/Spirulina microalgae composites, Macromol. Res. 25 (2017) 165–171, https://doi.org/10.1007/s13233-017-5025-9.
[3] S. Paneer Selvam, S. Ayyappan, S. I Jamir, L.Kumar Sellappan, S. Manoharan, Recent advancements of hydroxyapatite and polyethylene glycol (PEG) composites for tissue engineering applications – A comprehensive review, Eur. Polym. J. 215 (2024) 113226, https://doi.org/10.1016/j.eurpolymj.2024.113226.
[4] M.M. Stevens, Biomaterials for bone tissue engineering, Mater. Today 11 (2008) 18–25, https://doi.org/10.1016/S1369-7021(08)70086-5.
[5] N. Jiang, W. Zhang, Z. Meng, D. Li, J. Li, J. Ma, J. He, Effect of in vivo implantation sites on the graft-to-bone osteointegration induced by gradient nanofibrous scaffolds, Appl. Mater. Today 35 (2023) 101969, https://doi.org/10.1016/j.apmt.2023.101969.
[6] K. Ren, Y. Wang, T. Sun, W. Yue, H. Zhang, Electrospun PCL/gelatin composite nanofiber structures for effective guided bone regeneration membranes, Mater. Sci. Eng. C. 78 (2017) 324–332, https://doi.org/10.1016/j.msec.2017.04.084.
[7] P. Vilanova-Corrales, E. Demiquels-Punzano, J. Caballé-Serrano, F. Hernández-Alfaro, J.A. Delgado, R.A. Pérez, J. Gil, L.M. Delgado, Biodegradable and reinforced membranes based on polycaprolactone and collagen for guided bone regeneration, Mater. Today Commun. 41 (2024) 111039, https://doi.org/10.1016/j.mtcomm.2024.111039.
[8] H. Guo, D. Xia, Y. Zheng, Y. Zhu, Y. Liu, Y. Zhou, A pure zinc membrane with degradability and osteogenesis promotion for guided bone regeneration: In vitro and in vivo studies, Acta Biomater. 106 (2020) 396–409, https://doi.org/10.1016/j.actbio.2020.02.024.
[9] J.-T. Yeh, W.-L. Chai, C.-S. Wu, Study on the Preparation and Characterization of Biodegradable Polylactide/SiO_2–TiO_2 Hybrids, Polym. Plast. Technol. Mater. 47 (9) (2008) 887–894, https://doi.org/10.1080/03602550802189076.
[10] S. Jin, R. Yang, C. Chu, C. Hu, Q. Zou, Y. Li, Y. Zou, Y. Man, J. Li, Topological structure of electrospun membrane regulates immune response, angiogenesis and bone regeneration, Acta Biomater. 129 (2021) 148–158, https://doi.org/10.1016/j.actbio.2021.05.042.
[11] R.V. Chernozem, O. Guselnikova, M.A. Surmeneva, P.S. Postnikov, A.A. Abalymov, B.V. Parakhonskiy, N. De Roo, D. Depla, A.G. Skirtach, R.A. Surmenev, Diazonium chemistry surface treatment of piezoelectric polyhydroxybutyrate scaffolds for enhanced osteoblastic cell growth, Appl. Mater. Today 20 (2020) 100758, https://doi.org/10.1016/j.apmt.2020.100758.
[12] R. Álvarez-Chimal, J.Á. Arenas-Alatorre, M.A. Álvarez-Pérez, Nanoparticle - polymer composite scaffolds for bone tissue engineering. A review, Eur. Polym. J. 213 (2024) 113093, https://doi.org/10.1016/j.eurpolymj.2024.113093.
[13] G. Dal Poggetto, U. D'Amora, A. Ronca, M.G. Raucci, A. Soriente, G. Gomez d'Ayala, P. Laurienzo, Chemical modification of PLA for the design of 3D printed nanocomposite scaffolds with enhanced degradability for bone tissue engineering. Polym, Comp (2025) 1–17, https://doi.org/10.1002/pc.29470.
[14] A.M. Yousefi, G.E. Wnek, Poly (hydroxyalkanoates): Emerging biopolymers in biomedical fields and packaging industries for a circular economy. Biomedi. Mater 3 (2025) 19–44, https://doi.org/10.1007/s44174-024-00166-4.
[15] S. Ansari, N. Sami, D. Yasin, N. Ahmad, T. Fatma, Biomedical applications of environmental friendly poly-hydroxyalkanoates, Int. J. Biol. Macromol. 183 (2021) 549–563, https://doi.org/10.1016/j.ijbiomac.2021.04.171.
[16] H. Zhao, Z. Cui, X. Wang, L.S. Turng, X. Peng, Processing and characterization of solid and microcellular poly (lactic acid)/polyhydroxybutyrate-valerate (PLA/PHBV) blends and PLA/PHBV/Clay nanocomposites. C, ompos B Eng. 51 (2013) 79–91, https://doi.org/10.1016/j.compositesb.2013.02.034.
[17] F. Donnaloja, E. Jacchetti, M. Soncini, M.T. Raimondi, Natural and Synthetic Polymers for Bone Scaffolds Optimization, Polym 12 (2020) 905–932, https://doi.org/10.3390/POLYM12040905.
[18] M. Mohammadalipour, M. Asadolahi, Z. Mohammadalipour, T. Behzad, S. Karbasi, Plasma surface modification of electrospun polyhydroxybutyrate (PHB) nanofibers to investigate their performance in bone tissue engineering, Int J. Biol. Macromol. 230 (2023) 123167, https://doi.org/10.1016/j.ijbiomac.2023.123167.
[19] E. Fukada, Y. Ando, Piezoelectric properties of poly-β-hydroxybutyrate and copolymers of β-hydroxybutyrate and β-hydroxyvalerate, Int. J. Biol. Macromol. 8 (1986) 361–366, https://doi.org/10.1016/0141-8130(86)90056-5.
[20] R. Chernozem, O. Guselnikova, M. Surmeneva, P. Postnikov, A. Abalymov, B. Parakhonskiy, N. De Roo, D. Depla, A.G. Skirtach, R.A. Surmenev, Diazonium chemistry surface treatment of piezoelectric polyhydroxybutyrate scaffolds for

enhanced osteoblastic cell growth, Eur. Polym. J. 20 (2020) 100758, https://doi.org/10.1016/j.apmt.2020.100758.
[21] R.V. Chernozem, I.O. Pariy, A. Pryadko, P.A. Bonartsev, V.V. Voinova, V. A. Zhuikov, T.K. Makhina, G.A. Bonartseva, K.V. Shaitan, V.V. Shvartsman, D. C. Lupascu, K.N. Romanyuk, A.L. Kholkin, R.A. Surmenev, M.A. Surmeneva, A comprehensive study of the structure and piezoelectric response of biodegradable polyhydroxybutyrate-based films for tissue engineering applications, Polym. J. 54 (2022) 1225–1236, https://doi.org/10.1038/s41428-022-00662-8.
[22] R. Turco, G. Santagata, I. Corrado, C. Pezzella, M. Di Serio, In vivo and post-synthesis strategies to enhance the properties of PHB-based materials: A review, Front. Bioeng. Biotechnol. 8 (2021) 619266, https://doi.org/10.3389/fbioe.2020.619266.
[23] W. Guo, K. Yang, X. Qin, R. Luo, H. Wang, R. Huang, Polyhydroxyalkanoates in tissue repair and regeneration, Eng. Regen. 3 (2022) 24–40, https://doi.org/10.1016/J.ENGREG.2022.01.003.
[24] L. Guo, Z. Liang, L. Yang L, W. Du, T. Yu, H. Tang, C. Li, H. Qiu, The role of natural polymers in bone tissue engineering, J. Control Rel 338 (2021) 571–582, https://doi.org/10.1016/J.JCONREL.2021.08.055.
[25] M.J. Silva, J.Y. Dias, A. Zaszczyńska, J.Rojas Robles, J. Abiade, T. Kowalczyk, D. Kołbuk, P.Ł. Sajkiewicz, A.L. Yarin, Biocomposite-based fibrous scaffolds of natural rubber/polyhydroxybutyrate blend reinforced with 45S5 bioglass aiming at biomedical applications, Polym. Compos 45 (2024) 1107–1127, https://doi.org/10.1002/pc.27839.
[26] Q. Zhao, X. Xu, T. Zheng, B. He, N. Zhang, D. Wang, J. Wei, Magnesium-phosphorus gel containing oxygen vacancy niobium oxide with photothermal property for treating tumor, preventing infection and facilitating bone generation, Biomater. Adv. 172 (2025) 214237, https://doi.org/10.1016/j.bioadv.2025.214237.
[27] N. Marins, B.E.J. Lee, R.M. Silva, A. Raghavan, N.L. Villarreal Carreño, K. Grandfield, Niobium pentoxide and hydroxyapatite particle loaded electrospun polycaprolactone/gelatin membranes for bone tissue engineering, Colloids Surf. B Biointerfaces (2019) 110386 https://doi/10.1016/j.colsurfb.2019.110386.
[28] S. Mallakpour, M. Dinari, Enhancement in thermal properties of poly(vinyl alcohol) nanocomposites reinforced with Al_2O_3 nanoparticles, J. Reinf. Plast. Comp. 32 (2013) 217–224, https://doi.org/10.1177/0731684412467236.
[29] R.L. Karlinsey, A.T. Hara, K. Yi, C.W. Duhn, Bioactivity of novel selfassembled crystalline Nb_2O_5 microstructures in simulated and human salivas, Biomed. Mater. 1 (2006) 16–23, https://doi/10.1088/1748-6041/1/1/003.
[30] E. Eisenbarth, D. Velten, M. Müller, R. Thull, J. Breme, Biocompatibility of β-stabilizing elements of titanium alloys, Biomat 25 (26) (2004) 5705–5713, https://doi.org/10.1016/j.biomaterials.2004.01.021.
[31] J. Ge, F. Wang, Z. Xu, X. Shen, C. Gao, D. Wang, G. Hu, J. Gu, T. Tang, J. Wei, Influences of niobium pentoxide on roughness, hydrophilicity, surface energy and protein absorption, and cellular responses to PEEK based composites for orthopedic applications, J. Mater. Chem. B. 8 (2020) 2618–2626, https://doi.org/10.1039/C9TB02456E.
[32] A.P. Heitmann, P.S. Patrício, I.R. Coura, E.F. Pedroso, P.P. Souza, H.S. Mansur, A. Mansur, L.C. Oliveira, Nanostructured niobium oxyhydroxide dispersed Poly (3-hydroxybutyrate)(PHB) films: Highly efficient photocatalysts for degradation methylene blue dye, Appl. Catal. B Environ. 189 (2016) 141–150, https://doi.org/10.1016/j.apcatb.2016.02.031.
[33] A.P. Heitmann Rodrigues, I.C. Rocha, A.C. Mottin, L. Carlos Alves Oliveira, P.S. de Oliveira Patrício, Use of poly (3-hydroxybutyrate)/niobium oxyhydroxide nanocomposites in photocatalysis: Effect of preparation methods, J. Appl. Polym. Sci. 135 (2018) 5836, https://doi.org/10.1002/app.45836.
[34] L. Chen, M.J.B. Wang, Production and evaluation of biodegradable composites based on PHB−PHV copolymer, Biomat 23 (2002) 2631–2639, https://doi.org/10.1016/S0142-9612(01)00394-5.
[35] S. Rabiej, A comparison of two X-ray diffraction procedures for crystallinity determination, Eur. Polym. J. 27 (1991) 947, https://doi.org/10.1016/0014-3057(91)90038-P.
[36] A. Valentino, R. Conte, I. De Luca, F. Di Cristo, G. Peluso, M. Bosetti, A. Calarco, Thermo-Responsive Gel Containing Hydroxytyrosol-Chitosan Nanoparticles (Hyt@tgel) Counteracts the Increase of Osteoarthritis Biomarkers in Human Chondrocytes, Antioxid. (Basel) 11 (6) (2022) 1210, https://doi.org/10.3390/antiox11061210.
[37] A. Calarco, A. Di Salle, L. Tammaro, I. De Luca, S. Mucerino, O. Petillo, F. Riccitiello, V. Vittoria, G. Peluso, Long-Term Fluoride Release from Dental Resins Affects STRO-1+ Cell Behavior, J. Dent. Res. 94 (8) (2015) 1099–1105, https://doi.org/10.1177/0022034515584615.
[38] A.A. Eze, E.R. Sadiku, W.K. Kupolati, J. Snyman, J.Musyoka Ndambuki, T. Jamiru, M.Olayinka Durowoju, I.David Ibrahim, M.Brendon Shongwe, Dawood A. Desai, Wet ball milling of niobium by using ethanol, determination of the crystallite size and microstructures, Sci. Rep. 11 (2021) 22422, https://doi.org/10.1038/s41598-021-01916-w.
[39] Z.F. Fu, P. Liu, X.M. Chen, J.L. Ma, H.W. Zhang, Low-temperature synthesis of $Mg_4Nb_2O_9$ nanopowders by high-energy ball-milling method, J. Alloy. Compd. 493 (2010) 441–444, https://doi.org/10.1016/j.jallcom.2009.12.122.
[40] G.P. Costa, R.A. Rafael, J.C.S. Soares, A.B. Gaspar, Synthesis and characterization of ZnO-Nb_2O_5 catalysts for photodegradation of bromophenol blue, Catal. Today 344 (2020) 240–246, https://doi.org/10.1016/j.cattod.2019.04.059.
[41] A.A. Ol'khov, O.V. Staroverova, M.A. Gol'dshtrakh, A.V. Khvatov, K. Z. Gumargalieva, A.L. Iordanskii, Electrospinning of biodegradable poly-3-hydroxybutyrate. Effect of the characteristics of the polymer solution, Russ. J. Phys. Chem. 10 (2016) 830–838, https://doi.org/10.1134/S1990793116050213.
[42] L.R. Nivedita, A. Haubert, A.K. Battu, C.V. Ramana, Correlation between crystal structure, surface/interface microstructure, and electrical properties of nanocrystalline niobium thin films, Nanomat 10 (7) (2020) 1287, https://doi.org/10.3390/nano10071287.
[43] V. Allizond, G. Banche, M. Salvoni, M. Malandrino, C. Cecone, A.M. Cuffini, P. Bracco, Facile one-step electrospinning process to prepare AgNPs-Loaded PLA and PLA/PEO mats with antibacterial activity, Polym 15 (6) (2023) 1470, https://doi.org/10.3390/polym15061470.
[44] F.M. Sánchez-Arévalo, L.D. Muñoz-Ramírez, M. Álvarez-Camacho, F. Rivera-Torres, A. Maciel-Cerda, R. Montiel-Campos, R. Vera-Graziano, Macro-and micromechanical behaviors of poly (lactic acid)–hydroxyapatite electrospun composite scaffolds, J. Mater. Sci. 52 (2017) 3353–3367, https://doi.org/10.1007/s10853-016-0624-y.
[45] M. Sadat-Shojai, Electrospun polyhydroxybutyrate/hydroxyapatite nanohybrids: microstructure and bone cell response, J. Mater. Sci. Technol. 32 (10) (2016) 1013–1020, https://doi.org/10.1016/j.jmst.2016.07.007.
[46] F. Zheng, S. Wang, S. Wen, M. Shen, M. Zhu, X. Shi, Characterization and antibacterial activity of amoxicillin-loaded electrospun nano-hydroxyapatite/poly (lactic-co-glycolic acid) composite nanofibers, Biomat 34 (2013) 1402–1412, https://doi.org/10.1016/j.biomaterials.2012.10.071.
[47] T. Furukawa, H. Sato, R. Murakami, J. Zhang, Y.X. Duan, I. Noda, S. Ochiai, Y. Ozaki, Structure, dispersibility, and crystallinity of poly (hydroxybutyrate)/poly (L-lactic acid) blends studied by FT-IR microspectroscopy and differential scanning calorimetry, Macromol 38 (15) (2005) 6445–6454, https://doi.org/10.1021/ma0504668.
[48] S. Mallakpour, A. Nezamzadeh, Polymer nanocomposites based on modified ZrO_2 NPs and poly(vinyl alcohol)/poly(vinyl pyrrolidone) blend: optical, morphological and thermal properties, Polym. Plast. Technol. 56 (10) (2016) 1136–1145, https://doi.org/10.1080/03602559.2016.1253741.
[49] J.S. Lim, K.I. Park, G.S. Chung, J.H. Kim, Effect of composition ratio on the thermal and physical properties of semicrystalline PLA/PHB-HHx composites, Mater. Sci. Eng. C. 33 (4) (2013) 2131–2137, https://doi.org/10.1016/j.msec.2013.01.030.
[50] C.Y. Tang, D.Z. Chen, C.P. Tsui, P.S. Uskokovic, P.H.F. Yu, M.C.P. Leung, Nonisothermal melt-crystallization kinetics of hydroxyapatite-filled poly(3-hydroxybutyrate) composites, J. Appl. Polym. Sci. 102 (2006) 5388–5395, https://doi.org/10.1002/app.25016.
[51] M.H. Ho, S.Y. Li, C.Y. Ciou, T.M. Wu, The morphology and degradation behavior of electrospun poly (3-hydroxybutyrate)/Magnetite and poly (3-hydroxybutyrate-co-3-hydroxyvalerate)/Magnetite composites, J. Appl. Polym. Sci. 131 (22) (2014) 41070, https://doi.org/10.1002/app.41070.
[52] S. Phongtamrug, K. Tashiro, X-ray Crystal Structure Analysis of Poly(3-hydroxybutyrate) β-Form and the Proposition of a Mechanism of the Stress-Induced α-to-β Phase Transition, Macromol 52 (2019) 2995–3009, https://doi.org/10.1021/acs.macromol.9b00225.
[53] W.J. Orts, R.H. Marchessault, T. l Bluhm, G.K. Hamer, Observation of strain-induced β form in poly(β-hydroxyalkanoates), Macromol 23 (1990) 5368–5370.
[54] H. Yamane, K. Terao, S. Hiki, Y. Kimura, Mechanical properties and higher order structure of bacterial homo poly(3-hydroxybutyrate) melt spun fibers, Polymer 42 (2001) 3241–3248, https://doi.org/10.1016/S0032-3861(00)00598-X.
[55] V.K. Balasubramanian, R. Chellapandi, M. Balakrishnan, K. Murugan, J.P.K. J. Kennedya, S. Murugan, M.V. Khumalo, P.K.S., J.-Y. Chou, J. B. Muthuramalingam, Biosynthesis of bioplastic polyhydroxybutyrate (PHB) from microbes isolated from paddy/sugarcane fields and fabrication of biodegradable thin film, Process Saf. Environ. Prot. 187 (2024) 1178–1188, https://doi.org/10.1016/j.psep.2024.05.021.
[56] H. Sato, M. Nakamura, A. Padermshoke, H. Yamaguchi, H. Terauchi, S. Ekgasit, I. Noda, Y. Ozaki, Macromol 37 (2004) 3763, https://doi.org/10.1021/ma049863t.
[57] G. Uzun, D. Aydemir, Biocomposites from polyhydroxybutyrate and bio-fillers by solvent casting method, Bull. Mater. Sci. 40 (2017) 383–393, https://doi.org/10.1007/s12034-017-1371-7.
[58] L.V. Scalioni, M.C. Gutierrez, M.I. Felisberti, Green composites of poly(3-hydroxybutyrate) and curaua fibers: Morphology and physical, thermal, and mechanical properties, J. Appl. Polym. Sci. 134 (2017), https://doi.org/10.1002/app.44676.
[59] K. Majerczak, D. Wadkin-Snaith, V. Magueijo, P. Mulheran, J. Liggat, K. Johnston, Polyhydroxybutyrate: a review of experimental and simulation studies of the effect of fillers on crystallinity and mechanical properties, Polym. Int. 71 (2022) 1398–1408, https://doi.org/10.1002/pi.6402.
[60] A.S. Pryadko, Y.R. Mukhortova, R.V. Chernozem, L.E. Shlapakova, D.V. Wagner, K. Romanyuk, E.Y. Gerasimov, A. Kholkin, R.A. Surmenev, M.A. Surmeneva, Comprehensive study on the reinforcement of electrospun PHB scaffolds with composite magnetic Fe3O4–rGO fillers: structure, physico-mechanical properties, and piezoelectric response, ACS Omega 7 (45) (2022) 41392–41411, https://doi.org/10.1021/acsomega.2c05184.
[61] M. Di Maro, M.G. Faga, G. Malucelli, F.D. Mussano, T. Genova, R.E. Morsi, A. Hamdy, D. Duraccio, Influence of chitosan on the mechanical and biological properties of HDPE for biomedical applications, Polym. Test. 91 (2020) 106610, https://doi.org/10.1016/j.polymertesting.2020.106610.
[62] A. Dorigato, A. Pegoretti, Y. Dzenis, Filler aggregation as a reinforcement mechanism in polymer nanocomposites, Mech. Mater. 61 (2013) 79–90, https://doi.org/10.1016/j.mechmat.2013.02.004.
[63] G.H. Michler, H.H. Kausch-Blecken von Schmeling, The physics and micro-mechanics of nano-voids and nano-particles in polymer combinations, –44, Polym 54 (2013) 3131, https://doi.org/10.1016/j.polymer.2013.03.035.

[64] N. Eliaz, Degradation of implant materials (ed), Springer Science & Business Media, 2012.
[65] O. Gil-Castell, J.D. Badia, J. Bou, A. Ribes-Greus, Performance of polyester-based electrospun scaffolds under in vitro hydrolytic conditions: From short-term to long-term applications, Nanomat 9 (5) (2019) 786, https://doi.org/10.3390/nano9050786.
[66] C. Zhou, Q. Shi, W. Guo, L. Terrell, A.T. Qureshi, D.J. Hayes, Q. Wu, Electrospun bio-nanocomposite scaffolds for bone tissue engineering by cellulose nanocrystals reinforcing maleic anhydride grafted PLA, ACS Appl. Mater. Interfaces 5 (9) (2013) 3847–3854, https://doi.org/10.1021/am4005072.
[67] E.I. Paşcu, J. Stokes, G.B. McGuinness, Electrospun composites of PHBV, silk fibroin and nano-hydroxyapatite for bone tissue engineering, Mater. Sci. Eng. C. Mater. Biol. Appl. 33 (2013) 4905–4916, https://doi.org/10.1016/j.msec.2013.08.012.
[68] X. Wang, L. Yuan, J. Huang, T.-L. Zhang, K.J. Wang, Lanthanum enhances in vitro osteoblast differentiation via pertussis toxin-sensitive gi protein and ERK signaling pathway, Cell. Biochem 105 (2008) 1307–1315, https://doi.org/10.1002/jcb.21932.
[69] M. Tamai, K. Isama, R. Nakaoka, T.J. Tsuchiya, Synthesis of a novel b-tricalcium phosphate/hydroxyapatite biphasic calcium phosphate containing niobium ions and evaluation of its osteogenic properties, Artif. Organs 10 (2007) 22–28, https://doi.org/10.1007/s10047-006-0363-y.
[70] A. Obata, Y. Takahashi, T. Miyajima, K. Ueda, T. Narishima, T. Kasuga, Effects of niobium ions released from calcium phosphate invert glasses containing Nb_2O_5 on osteoblast-like cell functions, ACS Appl. Mater. Interfaces 4 (10) (2012) 5684–5690, https://doi.org/10.1021/am301614a.
[71] J. Zhang, C. Liu, Y. Li, J. Sun, P. Wang, K. Di, H. Chen, Y. Zhao, Effect of yttrium ion on the proliferation, differentiation and mineralization function of primary mouse osteoblasts in vitro, J. Rare Earths 28 (3) (2010) 466–470, https://doi.org/10.1016/S1002-0721(09)60135-6.
[72] M.-Y.- Shie, S.-J. Ding, H.-C. Chang, The role of silicon in osteoblast-like cell proliferation and apoptosis, Acta Biomater. 7 (2011) 2604–2614, https://doi.org/10.1016/j.actbio.2011.02.023.
[73] M. Ikeuchi, A. Ito, Y. Dohi, H. Ohgushi, H. Shimaoka, K. Yonemasu, T.J. Tateishi, Biomed Mater. Res 67A (2003) 1115–1122, https://doi.org/10.1002/jbm.a.10041.
[74] J. Tan, J. Li, B. Cao, J. Wu, D. Luo, Z. Ran, L. Deng, X. Li, W. Jiang, K. Xie, L. Wang, Y. Hao, Niobium promotes fracture healing in rats by regulating the PI3K-Akt signalling pathway: An in vivo and in vitro study, J. Orthop. Transl. 13 (37) (2022) 113–125, https://doi.org/10.1016/j.jot.2022.08.007.
[75] N.H. Marins, R.M. Silva, C.P. Ferrua, D. Łukowiec, A.M. Barbosa, J.S. Ribeiro, F. Nedel, E.R. Zavareze, T. Tański, N.L.V. Carreño, Fabrication of electrospun poly (lactic acid) nanoporous membrane loaded with niobium pentoxide nanoparticles as a potential scaffold for biomaterial applications, J. Biomed. Mater. Res B Appl. Biomater. 108 (4) (2020) 1559–1567, https://doi.org/10.1002/jbm.b.34503.